energies

MDPI

Review

Advances in Cryogenic Fracturing of Coalbed Methane Reservoirs with LN_2

Sotirios Nik. Longinos [1,*], Lei Wang [1,2] and Randy Hazlett [1]

[1] Department of Petroleum Engineering, Nazarbayev University, Nur-Sultan 010000, Kazakhstan
[2] College of Energy, Chengdu University of Technology, Chengdu 610059, China
* Correspondence: sotirios.longinos@nu.edu.kz

Abstract: Coalbed methane (CBM) is a significant unconventional natural gas resource existing in matrix pores and fractures of coal seams and is a cleaner energy resource compared to coal and crude oil. To produce CBM, stimulation operations are required, given that the coal permeability is generally too low. Hydraulic fracturing is the most widely used technology for reservoir stimulation; however, there are a few challenging issues associated with it, e.g., huge water consumption. In the past decade, the use of liquid nitrogen (LN_2) as a fracturing fluid has been intensively studied for stimulating CBM reservoirs, achieving considerable progress in understanding fracturing mechanisms and optimizing fracturing techniques. This paper presents a thorough review of experimental design and observations, modeling procedures and results, field applications, and published patents. Existing studies are divided into five different groups for discussion and comparison, including immersion tests, injection tests, jet drilling tests, numerical modeling, and field applications. Based on the comprehensive evaluation of the outcomes, it is obvious that cryogenic fracturing using LN_2 is a promising eco-friendly fracturing technique that can effectively enhance coal rock permeability to increase the production of CBM.

Keywords: cryogenic fracturing; coalbed methane; immersion tests; injection experiments; numerical modeling

Citation: Longinos, S.N.; Wang, L.; Hazlett, R. Advances in Cryogenic Fracturing of Coalbed Methane Reservoirs with LN_2. *Energies* **2022**, *15*, 9464. https://doi.org/10.3390/en15249464

Academic Editor: Shu Tao

Received: 28 September 2022
Accepted: 10 November 2022
Published: 14 December 2022

1. Introduction

In 2020, the total amount of the world's energy consumption was 556.63 exajoules, 83.1% of which were provided by hydrocarbons [1,2], and the status will not vary crucially in coming years [3,4]. Coalbed methane, as an unconventional resource of natural gas [5], has seen its production increase to 1.4×10^{14} m^3, which accounts for approximately 20% of global natural gas resources [6]. While coal can be extensively fractured, the production of coalbed methane can be assisted tremendously by the creation of fractures emanating from and leading to wells that serve as the gathering system. Water is the primary power fluid for induced fracturing. The initial test in hydraulic fracturing took place in 1947, and the first industrial trial occurred in 1949 [7]. One problem with extracting CBM with conventional hydraulic fracturing is the consumption of large quantities of water, which brings about critical concern in arid regions. In addition, the accidental breakthrough of fluid during hydraulic fracturing operations can generate contamination to underground aquifers and the surrounding area, with many adverse consequences for the environment. Other negative consequences of the use of conventional hydraulic fracturing are serious formation damage and productivity loss, along with waste disposal [8–10]. Consequently, waterless fracturing methods would be a welcome solution from an ecological perspective. Oil-based and CO_2 energized oil fracturing, propellant and explosive fracturing, gas fracturing, gelled alcohol and liquefied petroleum gas fracturing, liquid/supercritical CO_2 fracturing, and LN_2 fracturing are possible alternatives [11–13].

Advantages in the use of LN_2 for fracturing include the elimination of water consumption without the need for chemical additives and the avoidance of formation damage.

Hence, LN_2 could be considered a candidate waterless fracturing fluid to stimulate CBM reservoirs [14–17]. Previous studies showed that the use of LN_2 augments the propagation of micro-cracks in specimens, resulting in the impairment of mechanical properties and in the amelioration of rock permeability. Furthermore, the porosity of wet coal specimens augmented with the increase of water saturation since LN_2 cooling leads to the enlargement of connections in water-filled cracks of coal [18–21].

Interest in LN_2 fracturing operations has been increasing among researchers over the last ten years. Until now, there have been no literature reviews explaining and comparing the outcomes of LN_2 fracturing in CBM reservoirs. This study systematically reviews laboratory methods for evaluating and illustrating the efficacy of LN_2 cryogenic fracturing for CBM reservoirs, modeling studies, and field pilots. Furthermore, we conducted critical discussions and proposed future research directions.

2. Laboratory Experimental Studies

Different modes have been developed to test the efficacy of the cryogenic treatment of rocks, and various analytical techniques have been adopted to characterize cryogenic fractures. Two modes of laboratory experimentation frequently used to test cryogenic fracturing processes are immersion tests [22] and injection tests [12]. In these tests, analytical and imaging methods were typically used, such as nuclear magnetic resonance (NMR), X-ray computer tomography scan (X-ray CT scan), scanning electron microscope (SEM), cryo-scanning electron microscope (cryo-SEM), and stereomicroscopic imaging. In this section, three cryogenic treatment modes are introduced, and the results obtained by fracture characterization techniques are illustrated.

2.1. Immersion Tests and Evaluation

In an immersion test, coal rock samples of relatively high temperature (from 50 °C to 100 °C) are partially or completely immersed into LN_2 to examine the fracturing capability of a LN_2 thermal shock. Immersion tests can be repeated several times on the same coal rock sample. That is, rock samples are first cooled down to the boiling point of LN_2, then warmed back to the original temperature, constituting one freezing and thawing cycle. Multiple cycles can be performed.

NMR is a technique extensively used for the characterization of pore size distributions and pore volumes in reservoirs [23]. NMR can test a greater range of pore sizes compared to other processes, such as optical microscopy (OM)-SEM-transmission electron microscopy (TEM) (qualitative analysis), small angle X-ray scattering (SAXS), small angle neutron scattering (SANS)-microcomputer tomography (μCT), and N_2 adsorption-CO_2 adsorption (quantitative analysis). It is a quick, developed, non-damaging, and handy process for examining the pore structure and range of pore magnitude of coal specimens. Hence, the alteration of pore structure in coal specimens before and after freezing–thawing cycles can be examined [24].

Cai et al. (2014) [25] conducted immersion tests for coal and sandstone specimens and characterized them using NMR. The specimens were first dried at 60 °C (coal) and 80 °C (sandstone) for 48 h and then were saturated for 48 h. Pore size distributions were then tested using NMR. Additional drying processes to obtain partial water saturations were carried out, with saturation determined by weight measurements. Finally, the specimens were submerged to LN_2 for different time periods. The outcomes showed that, in all coal samples, T_2 amplitudes augmented after LN_2 treatment. More specifically, the pore structure of specimens indicated enlargement after the use of LN_2, and the bigger pores corresponding to $T_2 > 33$ ms indicated increasing alteration with water saturation, with an exception for $S_w = 100\%$). However, sandstone specimens showed different behaviors with respect to water saturation. There was a downward trend in T_2 distribution after immersion tests in sandstones at low saturation, while specimens with water saturation from 30% to 70% showed an increasing augmentation in T_2 amplitude. Nonetheless, for T_2

greater than 33 ms, there was a reduction in amplitude. On the other hand, samples with a water saturation of 100% experienced a significant increase.

The NMR relaxation time is sensitive to the surface-to-volume ratio of a sample, which, in turn, can be related to a characteristic pore size and shape factor as

$$\frac{1}{T_2} = \rho_2 \left(\frac{S}{V}\right)_{pore} = F_S \frac{\rho_2}{r_c} \quad (1)$$

where T_2 is transverse relaxation time (ms), ρ_2 is a factor expressing the relaxation surface strength (μm/ms), $(S/V)_{pore}$ is the ratio of pore surface to volume (cm^{-1}), F_s is the shape factor, and r_c is the pore size. Furthermore, NMR outcomes indicated that after LN_2 treatment, coal specimens had more significant alterations compared to sandstone specimens, while there was amelioration in the pore space connected with free water in all water-containing coal specimens [25]. Figure 1 shows both the measured T_2 distributions of fully water-saturated specimens before and after freezing.

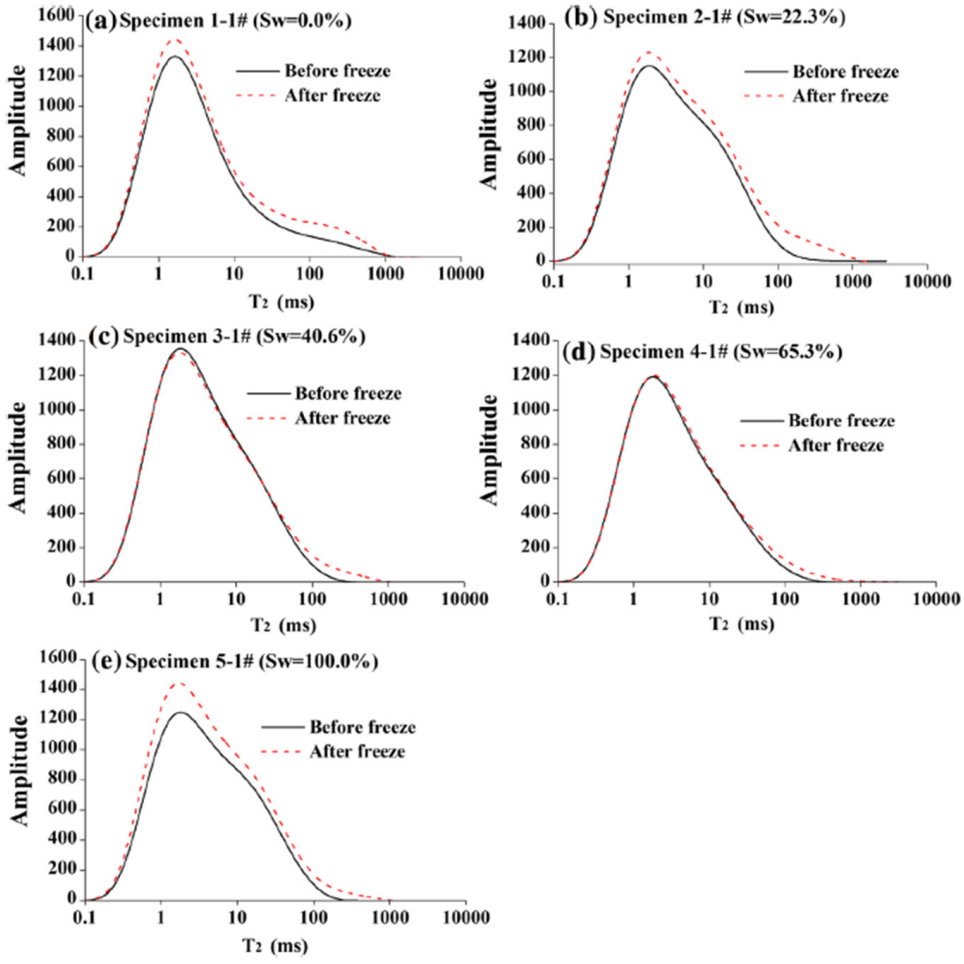

Figure 1. T_2 distributions for coal samples before and after freezing with LN_2.

Cai et al. (2015) [18] examined uniaxial compression before and after LN_2 treatment. Their outcomes showed that thermal stress caused a greater reduction in stress–strain curves compared to specimens without thermal shock, indicating the augmentation of micro-fracturing in specimens with LN_2. The compressive strength of specimens with the use of LN_2 was reduced from 16.18% to 33.74% compared with intact specimens. Moreover, the LN_2 treated specimens possessed more distinct brittle characteristics, and the largest reduction in axial peak was 20.61%. Furthermore, they examined the permeability of the samples before and after exposure to LN_2, indicating improvements of 48.89–93.55%. There

were more open fractures after the use of LN_2 compared to intact specimens. Furthermore, LN_2 shrank the coal matrix to generate thermal stress; hence, there was cracking of intergrain cementation and creation of local stress concentration at the tip of pre-existing cracks. With the augmentation of cracks inside the specimen, pore structure connectivity was greater, which translated into an augmentation in permeability [18]. Cai et al. (2016) [26] also compared coal and shale samples after immersion into LN_2. Their outcomes showed that the permeability of coal and shale samples augmented significantly after LN_2 cooling, confirming that LN_2 could promote the expansion of micro-cracks and induce rock fracturing [26].

Zhai et al. (2016) [14] examined coal samples from the Shengli coal mine in Inner Mongolia (China) using the processes of freezing and freezing–thawing cycles. They first dried the coal samples in the oven at 60 °C. Then, the samples were submerged in a water saturation device for 12 h operating under a vacuum to eliminate air in the system. The specimens were then treated by LN_2 freezing-thawing. Later, the specimens were resaturated before magnetic resonance image (MRI) analysis was carried out. Finally, the coal samples were centrifuged for 90 min to expel water within the connective macropores. According to T_2 curves, the widths and amplitudes for water-saturated specimens show a positive correlation with LN_2 freezing time. Moreover, the number of pores and freely connected pores increased with both the freezing time and the number of freezing–thawing cycles. On the other hand, the centrifuged specimens indicated a negative relationship between T_2 amplitude and freezing time, while the widths showed no changes, confirming that the number of closed pores reduced as freezing time increased [14].

Examining the porosity evolution and quantification after the use of LN_2, the outcomes suggested that the $T_{2cutoff}$ value and residual porosity reduce as the total porosity and effective porosity augment. The indication is that the number of fractures in coal increases after the use of LN_2 in the freezing–thawing process, and the augmented pore space gave the opportunity for CBM to desorb from the coal. The relationships between residual, total, and effective porosity are defined through the inclusion of free and bound fluid indices.

$$\varphi N_B = \varphi_N \times \frac{BVI}{BVI + FFI} \quad (2)$$

$$\varphi_{NF} = \varphi_N \times \frac{FFI}{BVI + FFI} \quad (3)$$

where φ_{NB}, φ_{NF} and φ_N are residual porosity, effective porosity, and total porosity, respectively. FFI and BVI are the free fluid index and the bound fluid index, respectively.

As quantified by the outcomes, the rate of change for both total ($\Delta\varphi_N$%) and effective porosity ($\Delta\varphi_{NF}$%) benefit from LN_2 freezing time and freezing–thawing cycles, while the residual porosity ($\Delta\varphi_{NB}$%) is influenced negatively by these elements.

$$\Delta\varphi = \varphi_{post} - \varphi_{pre} \quad (4)$$

$$\Delta\varphi\% = \frac{\Delta_\varphi}{\varphi_{pre}} \quad (5)$$

where $\Delta\varphi$ represents the porosity increment given by φ_{pre} and φ_{post} before and after the coals were then frozen and thawed, respectively. $\Delta\varphi$% is the rate of change in porosity under different freezing–thawing conditions. Furthermore, the incremental rates of the three porosities (total, residual, and effective) are linearly related to freezing time. On the other hand, in the freezing–thawing process, the rates showed nonlinear behavior. Specifically, as the number of freezing–thawing cycles increased, the alteration range of the porosity increment rate increased.

Zhai et al. (2016) [14] examined and described alterations in the number of pores versus freezing–thawing cycles. Dt expresses the rate of alteration in terms of the number of pores per unit volume of a coal specimen in T_2 spectrum area.

$$D_t = \frac{\Delta S}{S_{pre}} = \frac{S_{pre} - S_{post}}{S_{pre}} \quad (6)$$

where S is the region under T_2, and S_{pre} and S_{post} are the relevant regions in T_2 spectra of specimen before and after freezing–thawing cycles. Concerning pore growth and freezing time, cyclic freezing–thawing produces enhanced alteration compared to a single freezing–thawing treatment. Freezing–thawing experiments assisted in the creation of large seepage pores [14].

Moreover, Zhai et al. (2016) [14] described the influence of freezing–thawing cycles in axial, hoop, and volumetric strains (ε_v) in the coal specimen.

$$\varepsilon_v = \varepsilon_a + 2\varepsilon_r \quad (7)$$

where ε_a and ε_r represent the axial and hoop strains, respectively.

According to volumetric strain, freezing–thawing cycles were separated into four different smaller periods: freezing shrinkage period I (frost power related to the phase change of water into ice in the cracks), frost heave period II (expansion of frost power due to vaporization of LN_2), second freezing shrinkage period III (solid-state cryoturbation in the specimen at very low temperatures), and final frost heave period IV (state of in situ stress, σ). Hence, the coal specimen's morphology can be distorted through the freezing–thawing cycle method. Specimens broke when water and ice created swelling stress greater than the tensile strength of coal [14]. Figure 2 shows the failure caused after freezing–thawing, along with stress analysis for the fractures in coal.

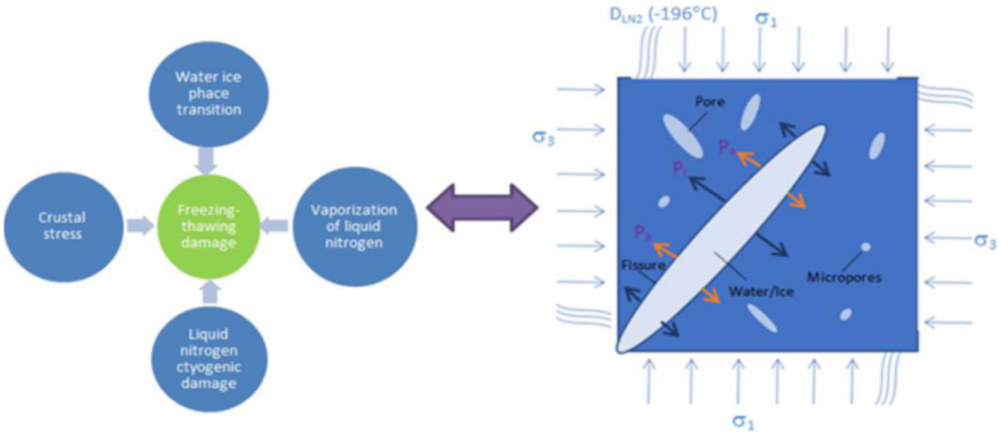

Figure 2. Schematic showing freezing–thawing damage caused by LN_2 and stress analysis for the fractures in coal [14].

Qin et al. (2016) [19] examined two sets of coal samples from the Shengli coal mine in Inner Mongolia (China) using the processes of freezing and freezing–thawing cycles at different moisture concentrations. Their outcomes indicated that the absolute values of axial and hoop strains diminished as the amount of freezing time, freezing–thawing cycles, and concentration of moisture increased. At the same time, the coal porosities were augmented by 17.5% and 68.1%, and Poisson's ratios by 7.14% and 28.6%, respectively. Due to the decrease in the coal's mechanical strength, the elastic strain stage was shortened, and the peak yield point and plastic deformation were accelerated. There was a negative relationship between uniaxial compressive strengths and elastic moduli with freezing time and freezing–thawing cycles, while the uniaxial compressive strengths and elastic moduli showed positive characteristics with increasing moisture content. Furthermore, the uniaxial

test outcomes were compatible with the acoustic emission outcomes [19]. Figure 3 shows the variations in the coal's elastic modulus and uniaxial compressive strength with the length of the freezing time and the number of freezing–thawing cycles.

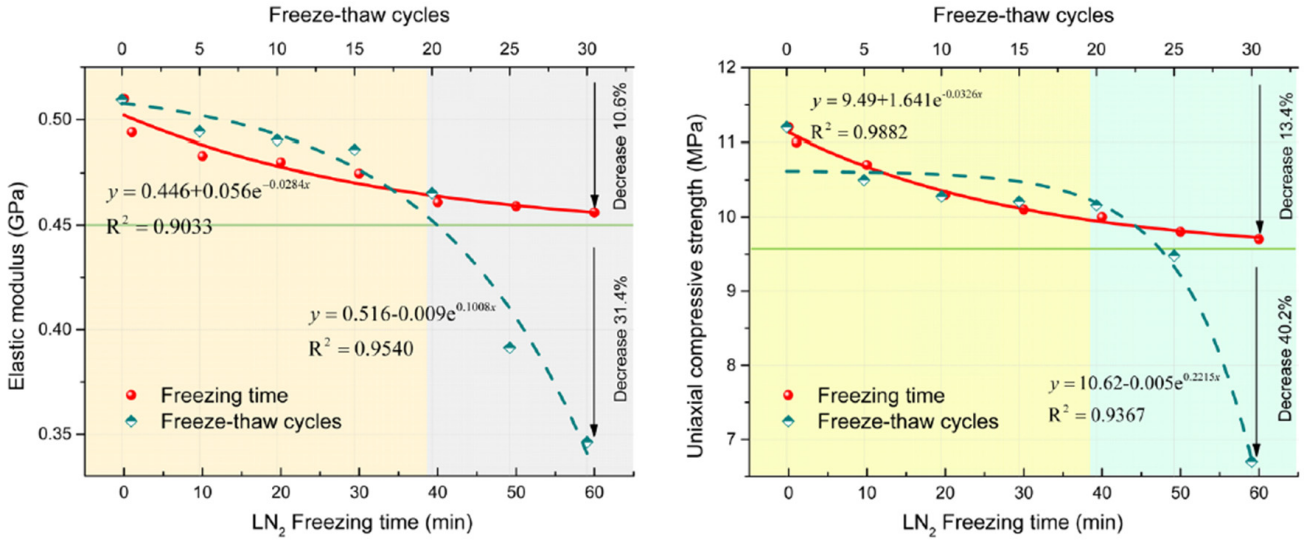

Figure 3. Changes in the elastic modulus and compressive strength after freezing–thawing cycles.

In addition, Qin et al. (2017a) [15] examined coal samples from Shengli (lignite), the Jungar (bituminous) coal mine in Inner Mongolia, and the Xinbei coalfield (anthracite) in Gansu, China. The first group of coal specimens was dried and then saturated with water. The samples were frozen and subjected to the freezing–thawing cycle process. The second group of experiments with different moistures (controlled by drying oven) were frozen for 90 min. Coal specimens of Shengli lignite were analyzed with different freezing times, different freezing–thawing cycles, and different moisture levels. The cyclic exposure samples were then put for vacuum saturation for 12 h. Finally, they were put in a centrifuge at 200 psi for 2 h. The results indicated that freezing time had a small influence on the permeability and porosity of the specimen. On the other hand, the number of freezing–thawing cycles imposed a great influence on pore structure. As the number of freezing–thawing cycles increased, porosity, and permeability were augmented, which is favorable for CBM extraction. As for samples containing moisture, the outcomes suggested that the greater the moisture concentration in coal specimens, the larger the increment of permeability. It should be mentioned that the influence of a high moisture concentration has limits. Comparing LN_2 freezing time effects and on lignite, anthracite, and bitumen, both the growth rate and total number of pores followed a downward trend of effectiveness: lignite > anthracite > bitumen. In contrast, the growth rate for seepage pores indicated a different behavior. The highest augmentation took place in anthracite, followed by bitumen, and then lignite. The influence of coal rank on the growth rates of porosity is also worth noting. The growth rates by rank, listed in downward trend, are lignite (low-rank), anthracite (middle-rank), and bituminous coal (high-rank). After the specimens were frozen and thawed using LN_2, the growth rates of their effective porosity and total porosity were all positive, but the growth rates of their residual porosity were negative. This means that after the coal samples were frozen and thawed, the closed pores were opened, and the open pores were augmented in magnitude and connectivity. This indicates improved reservoir conditions for extracting CBM [15].

They also went further to examine permeability after freezing–thawing cycles with the use of porosity parameters and the T_2 spectrum as a surrogate for pore size. They used three different models: the Schlumberger Doll Research (SDR) model, the Timur–Coates model, and the Producible Porosity model. The last two models indicated high error values; hence, only the outcomes of the SDR model were analyzed. Coals of disparate ranks show

different increments of permeability augmentation due to different initial coal porosity. The downward trending permeability enhancement created by LN_2 treatments, in order, is lignite, anthracite, and bituminous coal. Qin et al. (2017a) [15] also used SEM analysis, apart from NMR. SEM images showed that with LN_2 freezing of 10 min, the largest crack width was 13.3 µm, while for samples following 30 freezing–thawing cycles, the largest crack width was 60 µm, suggesting that the length and width of cracks augmented with freezing time or freezing–thawing cycles. LN_2 treatments also improved the fracture density per volume of specimens [19]. Furthermore, it was observed that the frost heaving influence of the water–ice phase transition first creates single primary cracks. Then, many other secondary cracks expand along the primary cracks. As the freezing–thawing cycles continue, the amplitude and complexity of the cracks slowly augment [15].

Qin et al. (2017b) [27] also analyzed the freezing–thawing damage variable, D,

$$D = 1 - \frac{E_n}{E_0} \tag{8}$$

where E_o and E_n are elastic moduli of the original and the frozen–thawed coal specimens.

Their outcomes through uniaxial stress analysis indicated that augmenting the freezing time brought the value of D up to about 0.12. On the other hand, moisture is negatively correlated with D, such that the smaller the moisture, the greater the damage done in the elastic deformation phase. Nevertheless, D values connected to moisture are curbed by a specimen's highest water saturation. Furthermore, fractal dimensions obtained using the box counting process on fractures rose from 1.06 to 1.23 for specimens undergoing 5 and 25 freezing–thawing cycles, respectively. The ultrasonic wave velocities indicated a negative connection with coal permeability, and cyclic freezing–thawing is efficient in augmenting coal permeability [27].

Li et al. (2018) [28] investigated coal specimens from the Yima Group, Henan Province. After freezing–thawing cycles, there was an observation of augmentation in permeability, pore diameter, and porosity in coal specimens. This augmentation became bigger in samples with water saturation greater than 70%. There was also an observation that thermal degradation dry specimens were due to cold shock, while in water-saturated specimens, apart from thermal degradation, water phase change is also responsible. They indicated that permeability enhancement pauses when the reduction of temperature extends to the maximum, mentioning that the progress of temperature reduction is connected to pore diameter, heat transfer properties, and freezing period [28].

Jin et al. (2019) [29] examined anthracite specimens of high metamorphism from Zhaogu No.1. Coal mine in Jiaozuo city and coking coal specimens of middle metamorphism from No.8 coal mine in Pingdingshan city and found that elastic modulus, compressive strength, and brittleness index are lower in specimens with LN_2 treatment compared to others without LN_2 treatment. For specimens with anthracite, the maximum strain of LN_2 cryogenic coal specimen augmented from 3.65% (non-cryogenic value) to 6.52%. For specimens with coking coal, the maximum strain of LN_2 cryogenic coal specimens increased from 4.75% (non-cryogenic value) to 5.69%. The average elastic modulus of LN_2 cryogenic anthracite was 1.75 GPa, which is lower than the average elastic modulus (2.48 GPa) of the non-cryogenic samples, with a reduction rate of 41.5%. The average elastic modulus of the coking coal samples diminished from 3.57 GPa to 1.75 GPa, with a reduction rate of 50.84% [29].

Chen et al. (2019) [30] examined bituminous coal samples from the Xutuan coal mine of Anhui province in China using the methods of freezing time and freezing–thawing cycles. Their outcomes indicated that a single LN_2 treatment under a stable confining pressure augmented permeability exponentially with the augmentation of gas injection pressure. On the other hand, freezing–thawing cycles initially caused reduction and then augmentation with increasing gas injection pressure. Furthermore, the permeability of coal specimens augments exponentially with the number of cycles, but the enhancement rate decreases slowly. Generally, LN_2 was successful in promoting the formation of macroscopic

fractures in coal and in increasing sample permeability. The level of damage to the coal structure under LN_2 circulation was much larger than that related to a single method, and the level of damage augmented with the number of cycles [30].

Chu et al. (2020) [24] examined anthracite coal samples from a Baijiao coal mine in China. Their tests started by drying samples for 24 h at 80 °C and then placing them in a water saturation device for 12 h with −0.1 MPa to achieve full saturation. They measured T_2 spectrum distribution and porosity through NMR. Finally, coal specimens were placed in a centrifuge machine at 200 psi pressure for 1.5 h to reach irreducible saturation. NMR examination was used again to estimate T_2 spectrum distribution and porosity. After these initial measurements, they compared freezing time and freezing thawing cycle methods at 60, 120, 180, 240, 300, and 360 min and 2, 4, 6, 8, 10, and 12 cycles (each freezing–thawing cycle comprised of 30 min of freezing and 30 min of thawing at room temperature), respectively. Outcomes indicated that with increasing length and number of freezing–thawing cycles, area, and amplitude of mesopores (100 nm to 1 μm) increased, inferring that considerable pore extension took place in micropores (<100 nm), which could turn into mesopores. The use of LN_2 can advance the link between pores, expedite the creation of fractures, significantly increase the ratio of mesopores to macropores (>1 μm), and notably augment the shape of seepage pores. Moreover, there is a tendency for stable enhancement with augmentation in freezing time and freezing–thawing cycles by the relative area change rate. The relative change area of the adsorption pores indicates an inclination for stable enhancement and then a steady reduction during LN_2 treatment, while the relative area change of the seepage pores shows an inclination for quick enhancement. Total porosity, effective porosity, and residual porosity were positively impacted by the use of LN_2 treatment time. There was also the observation that micropores constantly extend and then link to create more mesopores, macropores, and fractures driven by expansion and frost heaving pressure. Permeability measurements showed a significant augmentation effect after 4 freezing–thawing cycles; hence, more LN_2 freezing–thawing cycles can enhance the permeability by generating a larger number of mesopores and macropores, as well as enhancing the connectivity of pores. Their SEM analysis showed that the pore structure of coal specimens was constantly impaired and defaced, while fractures were created on the surfaces of the specimens. Increasing time and cycles, the cracks extended with an obvious increase in depth and width. New cracks created close to the initial ones can form a crack network by linking them to each other [24].

Du et al. (2020) [31] compared coal samples from the Yulin coal mine in Shanxi, China, and sandstone samples from Sichuan, China. The samples were dried for 12 h at 60 °C, weighted, and evaluated for P-wave velocity (V_p). The samples were submerged into LN_2 for 60 min and then analyzed. The results indicated that the micropores slowly expanded and linked with each other to create a network, augmenting the permeability in all coal samples. The use of LN_2 created both vertical and parallel fractures on coal surfaces; however, no obvious fractures took place on sandstone surfaces. This outcome showed that thermal stress compromised the integrity of the coal specimens by creating fractures. Hence, LN_2 is more effective in coal fracturing than sandstone fracturing [31], which was confirmed by Cai et al. (2014) in their NMR analysis [25]. Du et al. (2020) [31] also used an ultrasonic technique to compare coal and sandstone samples after the use of LN_2. Differentiation in wave velocities relates to the creation of new crevices or extending pre-existing crevices in rock specimens [32]. Broadly, waves of sound spread more quickly in solids than in liquids or gaseous. Hence, when V_p diminishes, more crevices may be created inside the rock specimen. After the use of LN_2, reduction in V_p was 24.7–38.1% with an average value of 30.63%, showing that the use of LN_2 had a beneficial effect in fracturing coal specimens. Furthermore, in one coal specimen, there was a great reduction in V_p, suggesting that large crevices may be created after the use of LN_2. On the contrary, V_p reduction for sandstone samples was only 0–0.06%, suggesting that LN_2 treatments of sandstone specimens created very little damage, which was also not visible [31].

Yan et al. (2020a) [10] examined coal samples from the Fenxi mining region of Shanxi, China. They followed an experimental process in which the coal sample was (a) heated to 60 °C in a drying oven for 24 h, (b) cooled to room temperature for 6 h, (c) examined by μCT scan, (d) immersed in LN_2 tank for approximately 1 h, and (e) equilibrated to room temperature for 30 min. Steps a to c were also repeated for the treated samples. The results indicated that LN_2 substantially influences pore distribution characteristics and strengthens their connectivity. According to stereoscopic diagrams, there was an augmentation of coal porosity by 183% after the use of LN_2. The surface porosity augmentation rate after thermal shocking is inversely related to the initial surface porosity of coal, suggesting that LN_2 fracturing is able to meet expectations for stimulating CBM reservoirs with low porosity and permeability. SEM analysis indicated that there were many deep and shallow scratch layers that showed progressive patterns. Moreover, several new cracks propagated, and sections of the pre-existing cracks extended and connected each other. Some embedded attachments are scoured, generating a few micro-holes or adventitious fractures on the surface. This fact affects the coal sample strength and could significantly ameliorate CBM reservoir recovery [10].

Su et al. (2020) [33] investigated coal specimens from a Yulin coal mine in Shanxi Province, China. Their outcomes showed that the tensile strength of coal samples under loading vertical and parallel to the coal bedding direction was reduced by 14.68% and 23.23%, respectively. Moreover, more complex fractures were observed following Brazilian splitting tests, while openings and the density of paths were also greater after LN_2 treatment. Lastly, SEM analysis suggested that amelioration in the permeability of a coal seam was due to multiple micro-cracks that were formed from matrix, original pores, and micro-cracks of coal after LN_2 treatment [33].

Akhondzadeh et al. (2020) [34] examined bituminous coal specimens from Morgantown, USA. The coal specimens were vacuum dried at 60 °C for 4 h in an oven. Then, the specimens were submerged in LN_2 for 60 min. The opening of the fractures before the use of LN_2 was not more than 10 μm, while after the treatment, an augmentation in the fracture aperture to 13 μm was noticed. Furthermore, it was observed that the created fractures were interconnected to the original cleats; hence, there was an augmentation in the apparent permeability of the specimen. According to the 3D analysis, the outcomes indicated that LN_2 not only created new fractures, but also interconnected the original isolated pores and fractures with the initial cleat network. SEM analysis performed in the pre-treatment and post-treatment states indicated that there were initially no important fractures in the SEM images of the specimen base and sides. After the use of LN_2, the largest crack opening was 9 μm. Furthermore, the fractures appeared on both sides and bases, forming a new fracture network inside the specimen. They also examined the mechanical properties of fracture rocks through nanoindentation. The indentation moduli, directly related to Young's modulus, of the specimen measured with 10 mN and 35 mN indentation forces were reduced by 5.1% and 14.4%, respectively. Such an important decrease corresponds to the existence of notably extended new fractures inside coal [34].

Zhang et al. (2020) [35] investigated the 3D microstructure and permeability changes in bituminous coal before and after LN_2 immersion. The outcomes indicated that accurate division of fractures was acquired, but that inordinate division could be avoided. Furthermore, according to the box-counting method, the 2D fractal dimensions of pore fractures in both directions augmented considerably after LN_2 treatment. The magnitude and quantity of fractures and crevices were augmented after LN_2 treatment. The summed volume of fractures augmented from 306.48 mm^3 to 967.55 mm^3, and the porosity augmented from 0.38% to 1.22%. Lastly, permeability values augmented exponentially with increasing inlet pressure under constant confining stress [35].

Zhang et al. (2020) [36] examined anthracite and bituminous coals subjected to both LN_2 cold shock and heating-cooling shock. Their specimens were from the Jiaozuo mining region of Henan province in China. Their results indicated a 2.11–3.89-fold improvement in permeability related to a sudden temperature increase from 180 °C to 360 °C. Their 3D

CT scan analysis indicated that thermal shocks increased the extension and linkage among fractures and effectively ameliorated the permeability of coal specimens. The results also indicated the formation of bifurcated and wing cracks on the surfaces of the coal samples during thermal shocks. The number of new cracks created by the heating–cooling method was greater than the single LN_2 cold shock. The crack propagation was also more complex in the heating-cooling method, indicating that the heating-cooling method achieved better outcomes in damaging and breaking the specimen than the cooling method alone [36].

Yan et al. (2020b) [13] examined coal specimens from the Zhongxing mine in Shanxi Province, China. They used two different samples with the same diameter of 25 mm and different heights of 42 mm and 50 mm for examining LN_2 quenching, along with various initial fracture magnitudes and saturations. The process was similar with LN_2 freezing–thawing cycle process with dry and water saturated specimens. Outcomes indicated that fracture thickness, fracture volume, fracture connectivity, and porosity augment with LN_2 freezing–thawing cycle process, notably, with the first cycle as the most significant. With the use of LN_2, large initial porosity was found to bear a smaller growth rate of surface porosity than small initial porosity, indicating greater prospects for the significant enhancement of rock specimens with low permeability. Furthermore, after the use of LN_2, there was continuous and gradual augmentation in the volume of fractures for the saturated coal specimens [13].

Lin et al. (2020) [37] examined coal specimens from the Hengyi Coal Mine in Shaanxi Province, China. They observed that fractures on the surface of coal specimens propagated after the use of LN_2. The authors reported expansion of fracture width with linear augmentation 3.3 times more with water-saturated specimens as compared to dried specimens. The damage factors expressed by fracture width, longitudinal wave velocity, and porosity were augmented exponentially. With the freezing–thawing cycle process, the longitudinal wave velocity in coal specimens was moderately reduced, and there was a positive exponential relationship between the decrease in wave velocity in coal specimens and the moisture concentration. Moreover, the freezing–thawing cycle process with LN_2 showed that micropores and small pores in coal mass were moderately changed to mesopores and macropores, in addition to the creation of new micropores and small pores [37].

Qin et al. (2020) [38] studied the pore size distribution of coal samples frozen by LN_2 with mercury porosimetery by combining the low-temperature nitrogen adsorption of lignite coal specimens from Shengli Coal Field, Inner Mongolia Autonomous Region, China. After freezing specimens for 180 min with LN_2, the number of small pores and macropores in the coal specimens increased. After 30 freezing thawing cycles, the quantity of small pores was reduced, but the number of macropores was augmented. Moreover, there is a beneficial exponential correlation with freezing time for both total pore volume and cumulative pore volume, but the augmentation gradually diminishes as freezing times augment. Nevertheless, the cumulative pore volume enhancement follows a quadratic function with the number of freezing–thawing cycles, and the increase slowly augments as the number of freezing–thawing cycles accrues [38].

Li et al. (2020) [39] studied anthracite coal samples collected from the Jiu Lishan Mine in Jiaozuo, China. According to their interpreted NMR results, there was augmentation in the number of small pores and micropores inside the coal specimens after LN_2 treatment. The water-saturated coal specimens had less thermal stress than the dried ones. The damage to water-saturated coal specimens was due to phase change, while in dry coal specimens, mechanical integrity was compromised due to thermal stress between particles. Generally, the temperature alteration of saturated coal is slower than that of dry coal, and the total to reaching equilibrium after thermal shock has a larger duration [39].

Liu et al. (2020) [40] collected samples from different regions. The specimens in the study were taken from the fat coal of the Pingmei No. 5 Coal Mine, the lean coal of the Daping Coal Mine, and the anthracite coal of the Guhanshan Coal Mine. The cryogenic nitrogen adsorption curves of the fat coal, lean coal, and anthracite before and after LN_2 cold soaking followed a lying "S" type. When $p/p_0 < 0.1$, there was a transition from monolayer

to multi-molecular layer adsorption, and the curve is convex. When $0.8 < p/p_0 < 1.0$, the adsorption curve is concave. Moreover, samples showed an enlargement in pores, mesopore volume and pore-specific surface area, total pore volume, and total pore-specific surface area for every coal specimen. Lastly, the thermal stress created during LN_2 treatment was larger than the tensile strength of coal. LN_2 treatment plays the role of augmenting and expanding the pore and advances the growth of the coal pore structure [40].

Akhondzadeh et al. (2021) [41] examined coal specimens using a multiscale tomographic study. Their outcomes indicated that in micro (μ-CT) and macro (medical CT) scales, LN_2 fracturing in anthracite specimens was poor. On the other hand, in bituminous and sub-bituminous specimens, porosity evolution augmented 14% and 119%, respectively. In macroscale bituminous and sub-bituminous specimens, there was substantial augmentation in their porosity. Connectivity assessment through skeletonization and Euler number analysis showed that sub-bituminous connectivity increased by 20-fold for small pores (<3 μm), while it doubled in bituminous [41].

Sun et al. (2021) [42] examined bituminous coal samples from the Datong coal mine in Shanxi province of China using the freezing–thawing cycle method. The process started by putting coal specimens in a vacuum saturator for 12 h to extract air to saturate with water. NMR analysis then took place. Later, the specimens were placed in a centrifuge at 8000 rpm for 1 h for the removal of free water, followed by further NMR analysis. Centrifugal specimens were dried for 12 h; then, ultrasonic emission and stereomicroscope image analyses were performed. The specimens were also saturated and then immersed in LN_2 for 10 min, followed by water bath (40 °C) immersion for 10 min. The outcomes indicated that the width and range of the T_2 curve in coal specimens were augmented. With a higher number of cold shock periods, total, and effective porosity, together with free fluid proportion, are augmented linearly, while both $T_{2cutoff}$ and residual porosity are reduced linearly. Furthermore, the contribution of micropores plays a leading role in the augmentation of effective porosity. The augmentation of open holes due to exposure to LN_2 was more advantageous for seepage and gas diffusion. They also analyzed fracture evolution by stereoscopy, observing that with increasing cold shock times, the surface porosity and the number of pores augmented, and the pore distribution movement tended to become more random. They concluded that short fractures in specimens slowly emerged, expanded, and extended to long fractures. As the secondary branch fractures expanded, ternary branch fractures formed and became visible. In the weak structural areas of the specimen, weak planes developed due to the high fracture density. A fracture network was created, and the specimen body was damaged. When the local weak area was totally damaged, a large amount of pulverized coal was generated. Furthermore, they also conducted ultrasonic wave analysis, indicating that, following the use of LN_2, there was a reduction in the amplitude of the first peak. The primary frequency of the ultrasonic wave diminished while the signal attenuation was augmented rapidly. The P-wave and S-wave velocities diminished gradually with the number of thermal socks. The structure of the coal specimen became layered instead of loose. Furthermore, the anisotropy augmented with the expansion of primary fractures but lessened with the creation of a primary-secondary fracture network. The dynamic mechanical parameters were reduced as the number of cold shocks increased, while the most crucial reduction took place in the dynamic bulk modulus [42].

Shao et al. (2021) [43] examined bituminous coal samples from the Tazigou coal mine in Liaoning, China. First, the samples were polished and put in a drying oven for 48 h at 45 °C. Then, half of the specimens were saturated with water. Furthermore, half the specimens from both groups were wrapped to investigate the impact of LN_2 on the physical and mechanical properties. Apart from cylindrical samples, there were also Brazilian discs tested at the same conditions. All the samples were submerged in LN_2 for 36 h and then allowed to warm to room temperature before starting the other measurements. SEM analysis of the saturated samples after the use of LN_2 indicated similar failure and crevice characteristics, with more significant damage than dry coal.

Nevertheless, interconnected fracture networks were created on the surfaces of the dry samples. Relatively short micro-fractures with low connectivity and narrow openings were created in the interior of dry coal specimens, notably without much penetration of LN_2. On the other hand, big failure regions and large fractures with connections were created in the interiors of the water-saturated specimens. P-wave velocity was also examined in all 4 different groups (water saturated wrapped and unwrapped, and dry wrapped and unwrapped). LN_2 reduced the P-wave velocity in all four groups. The impact order from high to low was: saturated wrapped specimen > saturated unwrapped specimen > dry unwrapped specimen > dry wrapped specimen. A higher cryogenic fracturing efficiency was observed in water-saturated specimens than in dry ones. Concerning gas permeability, there was significant augmentation in all four groups [43].

Lin et al. (2021) [44] examined the use of LN_2 in coal specimens from thermodynamic perspectives. The experiments started by drying 10 g of coal particles at 353 °K for 6 h in an oven. Then, the coal specimen was placed in a sealed freezing–thawing tank to return to room temperature. LN_2 was added to the system, and the tank was put in an oven for 2 h until the specimens returned to room temperature. After the freezing–thawing process, the oven was turned off, and coal specimens remained in a sealed container for 6 h until returning to room conditions (i.e., the completion of 1 cycle). After the appropriate number of freezing–thawing cycles, the specimen was again put in an oven and dried at 353 °K for 6 h to totally evaporate the free water created in the coal specimen during the freezing–thawing process. Then, the frozen–thawed specimen was weighed and placed into a high-pressure adsorption chamber, where the specimen was degassed by a vacuum pump, and helium was injected to estimate the fixed volume. By setting the specific experimental temperature, the maximum experimental pressure was 5 MPa, the pressure gradient was 1 MPa, and the system was filled by CH_4. When the experimental pressure equaled the set pressure and adsorption reached equilibrium, the experimental process terminated. The above steps were implemented to complete CH_4 adsorption experiments for coal specimens with different freezing–thawing cycles at different temperatures. Outcomes showed that the freezing–thawing process can obviously augment the CH_4 adsorption quantity of a coal specimen ($V_{unfrozen} < V_{freezing\ 5\ cycles} < V_{freezing\ 10\ cycles}$). The adsorption enthalpy H^{θ}, adsorption entropy S^{θ} and adsorption Gibbs free energy G^{θ} all increased as the freezing–thawing process continued. With the use of LN_2, the isosteric heat adsorption augments, because the LN_2 freezing–thawing process can greatly expand the adsorption sites of coal specimens. Furthermore, the heterogeneity of the coal specimen matrix augmented with the freezing–thawing process of LN_2. As the number of freezing–thawing cycles increased, the quantity of larger pores was augmented. The shedding of particles on the coal specimen surface and the extension of microchannels shows propitious signs for CBM adsorption [44].

Liu et al. (2021) [45] examined the effect of different LN_2 soaking times on the temperature distribution of coal specimens and explored the temperature evolution mechanism of anthracite-lignite-bituminous coals. Their experimental process was described as follows: the dried coal specimens were placed in an incubator at the same distance from a LN_2 injection hole. LN_2 was injected into the incubator through the hole until the coal specimen temperature stabilized. There were measurements taken to characterize coal specimens, and the process was repeated with alternative LN_2 soaking times. The outcomes indicated that with increasing LN_2 soaking times, the temperature of all three coal specimens exhibited three phases, including a reduction in their acceleration initially, continuation with small decline, and then stabilization at low temperature. The order to reach phase III (anthracite > bituminite > lignite) was opposite compared to the temperature-changing rate. Furthermore, thermal stress created in coal specimens helped in the extension and expansion of crevices and accelerated heat transfer. The temperature increase curve of the three coal specimens was augmented with time as a logarithmic function and indicated a unimodal distribution [45].

Qin et al. (2021) [46] investigated the effect of LN_2 on coals of different ranks (anthracite, lignite, bituminite) and gas adsorption. After 3 h immersion of samples in LN_2, outcomes indicated that the greatest amounts of adsorbed gas took place in lignite and bituminite, while the anthracite specimen showed a reduction. Furthermore, the contact angle for the anthracite specimen also decreased. The gas adsorption capacities of the specimens indicated a positive linear relation with the analogies of aliphatic hydrocarbon but a negative linear relation with the analogy of substituted benzene functional groups and oxygen-comprising functional groups. As the contact angles became greater, the coal gas adsorption capacities initially decreased but then augmented [46].

Sun et al. (2021) [47] examined coal specimens from Qinshui coal in China. They used the immersion method with SEM and NMR analyses. The initial NMR porosity of deep coal was smaller than that of shallow coal from the same coalfield and coal seam. There was an improvement in connectivity between mesopores and macropores in both deep and shallow specimens after the freezing–thawing cycle process. Furthermore, the quantity of micropores in the total pore structure volume diminishes, and the quantity of mesopores and macropores in the total pore structure volume accrues [47].

Yang et al. (2021) [48] developed a non-destructive geophysical technique using seismic measurements to probe fluid flow through coal and ascertain the effectiveness of cryogenic fracturing. Their results showed that the ultrasonic velocity of dry and saturated coal samples reduced overall with freezing time because of induced thermal and frost failure. For a gas-filled sample, both normal and shear fracture stiffness were reduced with freezing time, as more cracks formed in the coal bulk. On the other hand, for water-filled samples, ice formation due to cryogenic treatment is guided to the bottom of coal bulk [48].

Qin et al. (2022) [49] selected bituminous coal from the Hengyi Coal Mine in Shaanxi, China. They studied the influence of various LN_2 freezing variables on mechanical properties. Their outcomes showed that the mechanical strength of samples can be augmented for a period up to 100 min in LN_2 treatment where tensile stress elastic modulus and uniaxial compressive elastic modulus were augmented by 30.1% and 54.6%, respectively. However, as freezing times augment, there will be a reduction in the mechanical properties of coal. The freeze enhancement factor, I, augmented with increased freezing time, while the damage factor, D, augmented exponentially as the number of freezing–thawing cycles increased [49].

Yuan et al. (2022) [50] investigated specimens from Huainan Coalfield and Qinshui Coalfield by examining adsorption and desorption from middle- and high-rank coal specimens. The curve shape outcomes showed that coal specimens were typically mesoporous. Comparing middle-rank and high-rank coal specimens in terms of pore volume and average pore size, the results showed that in middle-rank coals, values were higher compared to high-rank coals [50].

Akhondzadeh et al. (2022) [51] investigated the LN_2 freezing–thawing process in coal fracturing, focusing on the influence of different freezing cycles examined in μ-Computed Tomography (μ-CT) images. The freezing–thawing process showed promising efficiency in cleat network evolution after three freezing–thawing cycles. The maximum opening of the initial fractures was 15 μm, while several new fractures had a maximum opening of 10 μm. According to connectivity analysis, the number of pores augmented 50%, while the number of interconnected pores almost doubled. SEM analysis indicated that there was creation of a fully penetrating fracture, which accrued in aperture magnitude and extended the cleat network of the specimen, especially in latter freezing–thawing cycles [51].

Hou et al. (2022) [11] examined coal specimens from the Yulin mining area of Shanxi Province. Their results indicated that coal after LN_2 treatment, in comparison with untreated specimens, increased compressive strength by 52.85%, in P-wave velocity 10.97%, in fracture toughness 495.07%, and in elastic modulus 38.76%. On the other hand, tensile stress decreased by 26.17%. Their outcomes were different in the freezing–thawing experiments. There was an important diminution for P-wave velocity of 26.14%, for elastic modulus 23.20%, for fracture toughness 58.33%, for compressive strength 21.20%, and for

tensile strength 42.99%. Micro-level outcomes showed that the failure mode, failure path, crack propagation direction, and fracture surface morphology of specimens in mechanical experiments became more complex, and the freezing–thawing specimens had the best failure effect [11].

Li et al. (2022) [52] selected coal specimens from the Qianjin coal mine in the Bijie coalfield, Guizhou, China. SEM outcomes indicated that as moisture content increased, the magnitude and width of pores augmented. NMR outcomes indicated that the proportion of micropores and transition pores from FT LN_2 treatment specimens was smaller than the untreated samples. Total pore volume, porosity, and average pore diameter were larger after LN_2 treatment. Moreover, permeability was increased after LN_2 treatment; the higher the moisture content, the higher the permeability of the coal samples after LN_2 treatment [52].

2.2. Injection Tests and Fracture Evaluation

LN_2 has been injected into the borehole drilled in a rock specimen to investigate its fracturing efficiency on the borehole wall. In most cases, confining stresses are exerted to mimic well stimulation scenarios under in situ stress conditions.

Cai et al. (2018) [53] examined coal specimens from Ordos in Inner Mongolia, China, using the method of LN_2 injection. A coal sample with a hole and injection tube was sealed with cement around it to make a cubic rock test specimen. Their acoustic emission (AE) outcomes indicated that as the specimens came into touch with LN_2, there was a continuous period of damage and cracking. The average AE ring-down count rate and cumulative ring-down counts during LN_2 injection were, at most, 14.45 and 12.08 times larger than before injection. Furthermore, the coal specimens had smaller tensile strengths than the specimens in their original state. In the cooling state, the specimens showed an average reduction of 17.39%, while in the cool-treated state, there was an augmentation of 31.43%. Reduction of wave velocity indicated that LN_2 can assist and expand the micro-fissures in the interior side of the specimen. In the cooling state, the average reduction in wave velocity was 14.46%, while in the cool-treated state, there was an augmentation of 18.68%. Additionally, during the LN_2 cooling process, AE signals were mainly produced from coal cracking [53].

After immersion tests with NMR and processing of SEM images, Qin et al. (2018) [54] continued to analyze the effect of LN_2 in CBM reservoirs with AE for both freezing and freezing–thawing injection methods. For the freezing injection method, the AE signals indicated that failure in the specimens took place near the injection tube and did not propagate. On the other hand, when they used the freezing–thawing injection, there was a plastic deformation region formed after the primary cracks were created and interconnected. Figure 4 shows the AE energy signals that were monitored during the single and cyclic LN_2 injections and the relationship between the AE energy and injection time.

Furthermore, after the use of LN_2 with a freezing time of 10,000 s and cyclic injection for 9 cycles for the same period, the lowest temperatures on the surface were -12 °C for the freezing method and -107 °C for cyclic injection method. In a single injection, the temperatures inside and outside the specimen ceased to diminish when they attained a specific value. Moreover, there was no effective fracture network in the tested specimens, and the heat transfer was through the solid material [54]. Mesoscopic analysis showed that the lower the density of the specimen, the higher the original water content, with larger associated frost heaving forces from water expansion during LN_2 injection. A greater temperature gradient forced more water to move, which resulted in more frost heaving due to water migration and ice accumulation. Furthermore, there was a connection between the shrinkage deformation of particles and the physical properties of the particles and a relationship between compression deformation and confining pressure [54].

Yin et al. (2018) [55] examined coal specimens from the Pingdingshan coal field of Henan Province, China, before and after the use of LN_2. Outcomes indicated that the micro-crevice threshold of coal specimens was far less than the frost heaving stress. Two main

changes that took place after the use of LN_2 were the nonuniform shrinkage deformation of coal specimens and the creation of pores, the majority of which were on the micropore and macropore scale. Concerning permeability, in low permeable and heterogeneous coal specimens, there was augmentation due to thermal cracking and sporadic opening of seepage pores due to phase change of free water in pores or micro crevices.

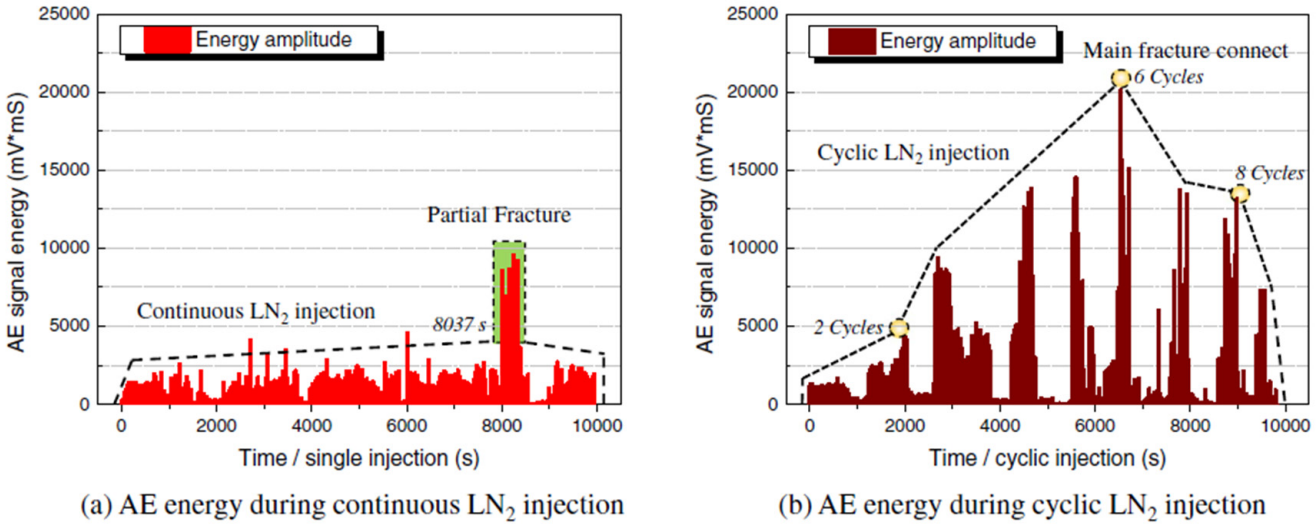

Figure 4. Changes in acoustic emission energy with time during the injection of LN_2.

Cong et al. (2021) [56] examined variations in the temperature field and strain field of coal around the drill hole after the injection of LN_2 into the drill hole. Upon heating from −30 °C to 30 °C, the expansion capacity augmented slowly until it leveled off. The average linear thermal expansion coefficient of coal in this temperature range was $\alpha = 36.06 \times 10^{-6}/°C$. Moreover, the low-temperature zone of coal around the drill hole expanded in a semicircular shape at a decelerated rate after LN_2 was injected into the drill hole. The strain and action range of frost contraction (long term) were larger than those of frost heave (short term) [56].

Yang et al. (2021) [57] examined synthetic coal cubes made of water, cement, sand, and coal particles with a ratio of 3:2:1:4. A 14-mm diameter, 3-mm thick stainless steel casing was then attached to the borehole with epoxy-resin adhesive. The casing extended 120 mm into the borehole, with an open-hole section of 60 mm. High pressure N_2 pressurized the LN_2 tank and pushed the LN_2 into boreholes under high pressure to perform the fracturing treatment. An insulation pipe was also applied between the high pressure LN_2 container and the borehole. The high pressure LN_2 tank can withstand a maximum pressure of 35 MPa and a minimum temperature of −196 °C. Moreover, there were also valves and fittings along LN_2 transportation lines that could withstand cryogenic conditions. In this research work, there was a comparison of LN_2 and water injection. Their outcomes indicated that the breakdown pressure for the LN_2-fractured specimen under higher confining stress may be lower than that for the water-fractured specimen subjected to a lower confining stress state. Furthermore, if the horizontal-stress-difference ratio is reduced from 1 to 0, the breakdown pressure of a specimen fractured by water will augment more considerably than that fractured by LN_2. The highly permeable regions were larger for LN_2-fractured specimens with multiple fractures starting from and adjacent to the borehole, while smaller stimulated areas were obtained in water-fractured samples, representing fractures with limited conductivity. The fracture planes of water-fractured samples were not as smooth as LN_2-fractured samples, and some of the water-fractured samples were not fully separated along the major fractures, showing that the fracture extension length was longer for LN_2 fracturing than water-based hydraulic fracturing. Hence, LN_2 fracturing tends to create more conductive and longer fractures than water fracturing. Concerning conductivity, the

fracture conductivity created by LN_2 fracturing can be 8 to 280 times as large as that by water fracturing. Their analysis with cryo-SEM enabled the imaging of specimens at a temperature of 190 °C and SEM analysis took place at room temperature. Comparing coal and sandstone samples, pre-existing pores in coal started creating fractures after the use of LN_2 with the maximum fracture width of 1.3 µm. On the other hand, there were no long fractures but only short cracks generated in sandstone specimens [57].

Du et al. (2021) [58] investigated coal specimens from the Zhang Minggou coal mine in Shaanxi, China. Their results showed that LN_2 cooling can cause significant thermal damage inside the coal, along with a reduction in P-wave velocity (approximately 15.8%). At the macroscopic level, the damage is stated as distortions in coal's mechanical properties, comprising tensile strength, peak strain, and absorbed energy. Lastly, the process of macrocrack propagation is closely related to the bedding angle [58]. Furthermore, the creation of cryogenic fractures or fissures on the surfaces of the coal specimens due to LN_2 were associated with the removal of some coal particles from the specimen's surface, which could act as self-propping agents to impede fracture closure in the thawing stage.

2.3. Jet Drilling

Jet drilling utilizes high-velocity fluids to break down rock samples of high strength. Water is the most used jet fluid. Recently, LN_2 has been tested as a jet fluid, seeing that thermal shock could boost its mechanical impact against rock specimens. Yang et al. (2019) [59] used a new method for CBM stimulation called Abrasive LN_2 Radial Jet Drilling (ALN-RJD), which drilled multiple radiating laterals instead of a single vertical wellbore to create more expanses in an eco-friendlier way. Their outcomes indicated that the coal-breakage threshold pressure of ALN-RJD was 87% and 89% of those of LN_2 jet and water jet, respectively. Furthermore, the pre-mixed abrasive LN_2 jets indicated better outcomes compared to post-mixed abrasive LN_2 jets in the field of coal breakage. ALN-RJD, due to its ability to create conductive pathways for gas transport in complex lateral-fracture networks, can augment cumulative gas production by 10% compared to the conventional RJD process. Thus, the greatest Net Present Value (NPV) could be achieved [59].

3. Modeling Studies

There have also been a few studies trying to simulate cryogenic fracturing processes. Cai et al. (2016) [26] simulated a LN_2 jet in abrading coal specimens using a computational fluid dynamics method to examine the effect of a LN_2 jet on particle removal along with cracking effects of LN_2 on coal specimens compared to a water jet. Simulation results indicated that under the same nozzle pressure difference, the LN_2 jet showed better conduct in abrasive particle removal and pressure boosting in the perforation cavity in coal than did the water jet. Furthermore, the impact influence caused by LN_2 was similar to that generated by water [26].

By integrating the Mogi–Coulomb failure criterion into TOUGH2-EGS (finite difference scheme), which couples thermal-hydraulic-mechanical processes, Yao et al. (2017) [60] successfully reproduced the bulb-shape fracture morphology generated by LN_2 treatment of boreholes in rock cubes and quantitatively matched the permeability enhancements.

Cai et al. (2018) also carried out temperature distribution simulations in rock samples. Their results indicated that even though the sample was subjected to injection by LN_2 for 850 s, the cement part around the coal remained at a relatively high temperature [53].

Along with immersion experimental studies, Jin et al. (2019) [29] examined LN_2 treatment in coal specimens using a strength statistical damage (SSD) constitutive model. Compared with the Mazars model, the SSD modeling reflects the stress–strain relationship of LN_2 cryogenic coal, which is consistent with experimental outcomes. Furthermore, the substantial causes for brittleness-ductility were cohesive force reduction and friction force augmentation [29].

Apart from the experimental study of abrasive jet drilling, Yang et al. (2019) [59] simulated a stimulated vertical CBM well located in the Horseshoe Canyon coals of Western

Canada. They modeled a rectangular reservoir with a dimension of 500 m × 500 m × 8.99 m, which was discretized into 100 × 100 × 1 grid blocks. The simulation time was 750 days. The RJD well indicated an amelioration in gas production rate of 65.8% at the end of the simulation period compared with the horizontal well. Furthermore, the cumulative gas production of the ALN-RJD well was 10.7% higher than that of the RJD well, showing that thermal crevices induced by the LN_2 jet played a significant role in production improvement [59].

The simulation results of Du et al. (2020) [31] demonstrated that the area with low temperature slowly expanded inside samples with time and created a tensile area in the samples. Moreover, in coal specimens, the heat transfer rate is lower than in sandstone specimens due to the higher thermal diffusivity of sandstone. The outcomes from a maximum normal stress calculation indicated that the maximum tensile stress created by momentary contact between coal and LN_2 was 3.41 MPa, while for sandstone samples, it was 4.87 MPa. This was probably because of the higher elastic modulus and thermal diffusivity values for the sandstone specimens. Finally, the simulation outcomes showed that the maximum failure region occurred 3.3 mm from the outer surface for coal specimens, while the failure region for sandstone specimens was almost zero, which confirmed the SEM and P-wave outcomes reviewed above in this work [31].

Cong et al. (2021a) [56] used a hierarchical model to calculate the thermal stress around a borehole. The absolute values of thermal stresses at the measuring points augment initially quickly and then increase steadily. Furthermore, the outcomes showed that thermal stress and thermal stress gradient are higher close to the drilled hole. The thermal stress was over 1.3 MPa and below 0.2 MPa. For the strain analysis results, the borehole underwent frost heave under the action of LN_2 cold shock (LNCS) on both sides. As the LNCS augmented, the frost heave area became the frost contraction area and kept expanding outward [60]. Moreover, Cong et al. (2021b) [61] used FLUENT software to show that the coal specimen side wall temperature quickly decreases and then levels out. Moreover, apart from the effect of a gas layer between the LN_2 interface and the coal specimen side wall, the low-temperature coal specimen side wall with high thermal resistance plays an important role in heat transfer [61].

Ma et al. (2021) [62] modeled the effective freezing radius during the LN_2 injection process. In a sample with a moisture content of 12%, the thermal conductivity of the coal sample was enhanced linearly with the reduction of temperature. The nearer to the freezing hole, the greater the temperature gradient of coal, but the temperature gradient reduced quickly at a certain distance. With an increment in the freezing time, the freezing front became larger outwards, but the rate of freezing front advancement was progressively reduced [62].

Wen et al. (2022) [63] developed a 3D, unsteady-state, fluid flow, and heat transfer model for LN_2 fracturing in a CBM reservoir, which considered the phase transition of nitrogen, thermophysical properties variation of coal, and the heat transfer between nitrogen and the formation. The outcomes indicated that thermal stress had a minor effect on the propagation of the primary fracture near the tip due to the small temperature difference. Moreover, the fracture aperture, injection velocity, reservoir temperature, injection fluid temperature, fracture propagation pressure, and coal cleat porosity affected the effectiveness of LN_2 fracturing in a coal seam [63].

4. Field Applications

Field applications of cryogenic fracturing are scarce and insufficient. Four CBM wells (A, B, C, and D) and one tight sandstone well (E) were stimulated with the use of LN_2 [64]. Well B was originally completed with nitrogen foam fracturing and had an average gas production of 85 Mcf/D in a period of 24 weeks before re-stimulation with cryogenic LN_2. After the use of LN_2 the initial production was 1600 Mcf/D at a 42% N_2 cut. The rate had then undergone a high reduction, and the well was produced sporadically. The rates for the next 16 weeks produced an average of 70 Mcf/D, while the rate after 12 months of the

use of LN_2 returned to approximately 85 Mcf/D. Well D had three attempts for stimulation, with the first two finished very early (first attempt with nitrogen foam and second with borate crosslinked gel). In the third attempt at stimulation, borate crosslinked gel was again used for better proppant transferring ability. Its gas production had an average of 42 Mcf/D in the period of 24 months before the use of LN_2. After LN_2 stimulation, the initial production rate was 400 Mcf/D while its average production rate was approximately 60 Mcf/D, indicating an amelioration of 43% [65].

It should also be mentioned that there are a few patents claiming case studies of cryogenic fracturing. The earliest patent referred to the recovery of methane gas from subterranean coal seams with the use of LN_2 to augment the permeability of the portion of a coal seam penetrated by a wellbore [65]. Zhang et al. (2016) [66] used LN_2 as a fracturing fluid and indicated that it is appropriate for the primary fracturing of non-fractured CBM wells and wells with existing natural fractures, as well as the re-fracturing of low productivity wells. Shen et al. (2017, 2018) [67,68] claimed that the LN_2 freezing–thawing method can effectively ameliorate a low-permeability coalbed; hence, the recovery of CBM can be improved. Zhai et al. (2018) [69] claimed a freezing–thawing procedure aimed at improving coal seam permeability by injecting LN_2 in a high-pressure pulsing manner. They indicated that its use is easy, practicable, and economically affordable. Furthermore, they claimed that their implementation could ameliorate both single-pore extraction and extraction concentrations of CBM, in addition to prolonging the attenuation time of gas concentration. Xu et al. (2020) [70] physically simulated LN_2 injection freezing–drying to augment the yield of CBM. They injected the LN_2 to fast freeze water in the coal briquette into ice to open gaps. Then, ice was heated to be directly sublimated into water vapor by combining vacuuming, which resulted in augmenting the yield of CBM.

5. Conclusions

During this transition time toward cleaner forms of energy and the push for eco-friendly solutions to conserve and protect fresh water, cryogenic fracturing with LN_2 offers distinct advantages over traditional water-based stimulation techniques in CBM exploitation.

Based on a thorough review of the use of LN_2 in stimulating CBM reservoirs, cryogenic fracturing can be an effective fracturing method for creating cracks and fracture networks in coal seams. Hundreds of experimental tests on coal demonstrated that existing fractures can be expanded and that new fractures can be initiated by LN_2, bringing about multifold permeability enhancement. Numerical modeling furthered our understanding of the cryogenic fracturing process by visualizing the distributions of temperature, stress, and the fractured region in a complementary manner. The limited number of field pilots carried out in coal seams 25 years ago can be considered successful, right after, despite the 15-year gap in research and development that followed. More recently, cryogenic fracturing has gathered momentum in terms of published research and case scenarios in patents.

Future studies recommended include fracturing mechanism revelation, simulation, large-scale experiments, and field pilot tests of LN_2 stimulation. In laboratory experiments, some cryogenic fractures may be too small for observation; hence, more advanced microscopy and fluorescence processes are imperative for the thorough characterization of thermal shock fractures. In addition, both freezing and thawing contribute to coal cracking; thus, optimization of their relative timings in a cycle deserves more effort. Moreover, more injection studies are recommended since almost 80% of research activities refer to immersion tests.

Additionally, simulation studies of cryogenic fracturing are limited. Thermal-hydraulic-mechanical processes should be coupled with fracturing criteria in simulators and scaled to design field pilot tests. In addition, thermal gradients, fracture formation and distribution, and the magnitude of permeability augmentation with cryogenic stimulation differ with specimen size. Hence, large-scale laboratory experiments using 1 cubic meter or more of coal or concrete/coal could be substantial for LN_2 delivery processes and advantageous audit tools for execution at the field scale. Cryogenic fractures partially close as temperature

returns to ambient, indicating that proppants are necessary to hold fractures open to maintain conductivity during or after a cryogenic stimulation treatment, both as experimental and as modeling studies. Apart from thermal effects, LN_2 has different compressibility and can evaporate; hence, future studies must also examine how these physical effects may contribute to the result, since evaporation can significantly increase the volume and create longer fractures. Another future focus area should be LN_2 viscosity and the ability to transport proppants.

Author Contributions: Conceptualization, S.N.L.; methodology, S.N.L.; software, S.N.L.; validation S.N.L. and R.H.; formal analysis, S.N.L.; investigation, S.N.L.; resources, S.N.L.; data curation, S.N.L.; writing—original draft preparation, S.N.L.; writing—review and editing, S.N.L.; visualization, S.N.L.; supervision, L.W. and R.H.; project administration, R.H.; funding acquisition, R.H. All authors have read and agreed to the published version of the manuscript.

Funding: This research was funded by NAZARBAYEV UNIVERSITY, grant number 021220CRP2022" and "The APC was funded by NAZARBAYEV UNIVERSITY.

Acknowledgments: The authors are thankful to Nazarbayev University, Kazakhstan, for financial support in the form of Collaborative Research Program grant: 021220CRP2022.

Conflicts of Interest: The authors declare no conflict of interest.

References

1. Longinos, S.N.; Parlaktuna, M. Examination of behavior of lysine on methane (95%)–propane (5%) hydrate formation by the use of different impellers. *J. Pet. Explor. Prod.* **2021**, *11*, 1823–1831. [CrossRef]
2. British Petroleum. *Statistical Review of World Energy*, 7th ed.; British Petroleum: London, UK, 2021.
3. Longinos, S.N.; Parlaktuna, M. Are the amino acids inhibitors or promoters on methane (95%)–propane (5%) hydrate formation? *React. Kinet. Mech. Catal.* **2021**, *132*, 795–809. [CrossRef]
4. Merey, Ş.; Longinos, S. The gas hydrate potential of the Eastern Mediterranean basin. *Bull. Miner. Res. Explor.* **2019**, *160*, 1–10. [CrossRef]
5. Tian, F.C.; Liang, Y.T.; Wang, D.M.; Jin, K. Effects of caprock sealing capacities on coalbed methane preservation: Experimental investigation and case study. *J. Cent. South Univ.* **2019**, *26*, 925–937. [CrossRef]
6. Crow, D.J.; Balcombe, P.; Brandon, N.; Hawkes, A.D. Assessing the impact of future greenhouse gas emissions from natural gas production. *Sci. Total Environ.* **2019**, *668*, 1242–1258. [CrossRef]
7. Liew, M.S.; Danyaro, K.U.; Zawawi, N.A.W.A. A Comprehensive Guide to Different Fracturing Technologies: A Review. *Energies* **2020**, *13*, 3326. [CrossRef]
8. Jackson, R.E.; Gorody, A.W.; Mayer, B.; Roy, J.W.; Ryan, M.C.; Van Stempvoort, D.R. Groundwater protection and unconventional gas extraction: The critical need for field-based hydrogeological research. *Groundwater* **2013**, *51*, 488–510. [CrossRef]
9. Boudet, H.; Clarke, C.; Bugden, D.; Maibach, E.; Roser-Renouf, C.; Leiserowitz, A. "Fracking" controversy and communication: Using national survey data to understand public perceptions of hydraulic fracturing. *Energy Policy* **2014**, *65*, 57–67. [CrossRef]
10. Yan, H.; Tian, L.P.; Feng, R.M.; Mitri, H.; Chen, J.Z.; Zhang, B. Fracture evolution in coalbed methane reservoirs subjected to liquid nitrogen thermal shocking. *J. Cent. South Univ.* **2020**, *27*, 1846–1860. [CrossRef]
11. Hou, P.; Su, S.; Gao, F.; Liang, X.; Wang, S.; Gao, Y.; Cai, C. Influence of Liquid Nitrogen Cooling State on Mechanical Properties and Fracture Characteristics of Coal. *Rock Mech. Rock Eng.* **2022**, *40*, 1–20. [CrossRef]
12. Wang, L.; Yao, B.; Cha, M.; Alqahtani, N.B.; Patterson, T.W.; Kneafsey, T.J.; Miskimins, J.L.; Yin, X.; Wu, Y.S. Waterless fracturing technologies for unconventional reservoirs-opportunities for liquid nitrogen. *J. Nat. Gas Sci. Eng.* **2016**, *35*, 160–174. [CrossRef]
13. Yan, H.; Tian, L.; Feng, R.; Mitri, H.; Chen, J.; He, K.; Zhang, Y.; Yang, S.; Xu, Z. Liquid nitrogen waterless fracking for the environmental protection of arid areas during unconventional resource extraction. *Sci. Total Environ.* **2020**, *721*, 137719. [CrossRef] [PubMed]
14. Zhai, C.; Qin, L.; Liu, S.; Xu, J.; Tang, Z.; Wu, S. Pore structure in coal: Pore evolution after cryogenic freezing with cyclic liquid nitrogen injection and its implication on coalbed methane extraction. *Energy Fuels* **2016**, *30*, 6009–6020. [CrossRef]
15. Qin, L.; Zhai, C.; Liu, S.; Xu, J.; Yu, G.; Sun, Y. Changes in the petrophysical properties of coal subjected to liquid nitrogen freeze-thaw–A nuclear magnetic resonance investigation. *Fuel* **2017**, *194*, 102–114. [CrossRef]
16. Ding, Z.; Jia, J.; Feng, R. Effect of the vertical stress on CO_2 flow behavior and permeability variation in coalbed methane reservoirs. *Energy Sci. Eng.* **2019**, *7*, 1937–1947. [CrossRef]
17. Memon, K.R.; Mahesar, A.A.; Ali, M.; Tunio, A.H.; Mohanty, U.S.; Akhondzadeh, H.; Awan, F.U.R.; Iglauer, S.; Keshavarz, A. Influence of cryogenic liquid nitrogen on petro-physical characteristics of mancos shale: An experimental investigation. *Energy Fuels* **2020**, *34*, 2160–2168. [CrossRef]
18. Cai, C.; Li, G.; Huang, Z.; Tian, S.; Shen, Z.; Fu, X. Experiment of coal damage due to super-cooling with liquid nitrogen. *J. Nat. Gas Sci. Eng.* **2015**, *22*, 42–48. [CrossRef]

19. Qin, L.; Zhai, C.; Liu, S.; Xu, J.; Tang, Z.; Yu, G. Failure mechanism of coal after cryogenic freezing with cyclic liquid nitrogen and its influences on coalbed methane exploitation. *Energy Fuels* **2016**, *30*, 8567–8578. [CrossRef]
20. Zhao, D.; Wang, Q.; Li, D.; Feng, Z. Experimental study on infiltration and freeze–thaw damage of water-bearing coal samples with cryogenic liquid nitrogen. *J. Nat. Gas Sci. Eng.* **2018**, *60*, 24–31. [CrossRef]
21. Qin, L.; Zhai, C.; Xu, J.; Liu, S.; Zhong, C.; Yu, G. Evolution of the pore structure in coal subjected to freeze− thaw using liquid nitrogen to enhance coalbed methane extraction. *J. Pet. Sci. Eng.* **2019**, *175*, 129–139. [CrossRef]
22. Cha, M.; Yin, X.; Kneafsey, T.; Johanson, B.; Alqahtani, N.; Miskimins, J.; Patterson, T.; Wu, Y.S. Cryogenic fracturing for reservoir stimulation–Laboratory studies. *J. Pet. Sci. Eng.* **2014**, *124*, 436–450. [CrossRef]
23. AlGhamdi, T.M.; Arns, C.H.; Eyvazzadeh, R.Y. Correlations between NMR-relaxation response and relative permeability from tomographic reservoir-rock images. *SPE Reserv. Eval. Eng.* **2013**, *16*, 369–377. [CrossRef]
24. Chu, Y.; Sun, H.; Zhang, D.; Yu, G. Nuclear magnetic resonance study of the influence of the liquid nitrogen freeze-thaw process on the pore structure of anthracite coal. *Energy Sci. Eng.* **2020**, *8*, 1681–1692. [CrossRef]
25. Cai, C.; Li, G.; Huang, Z.; Shen, Z.; Tian, S. Rock pore structure damage due to freeze during liquid nitrogen fracturing. *Arab. J. Sci. Eng.* **2014**, *39*, 9249–9257. [CrossRef]
26. Cai, C.; Huang, Z.; Li, G.; Gao, F.; Wei, J.; Li, R. Feasibility of reservoir fracturing stimulation with liquid nitrogen jet. *J. Pet. Sci. Eng.* **2016**, *144*, 59–65. [CrossRef]
27. Qin, L.; Zhai, C.; Liu, S.; Xu, J. Factors controlling the mechanical properties degradation and permeability of coal subjected to liquid nitrogen freeze-thaw. *Sci. Rep.* **2017**, *7*, 3675. [CrossRef]
28. Li, B.; Zhang, L.; Wei, J.; Ren, Y. Pore damage properties and permeability change of coal caused by freeze-thaw action of liquid nitrogen. *Adv. Civ. Eng.* **2018**, *2018*, 5076391. [CrossRef]
29. Jin, X.; Gao, J.; Su, C.; Liu, J. Influence of liquid nitrogen cryotherapy on mechanic properties of coal and constitutive model study. *Energy Sources Part A Recovery Util. Environ. Eff.* **2019**, *41*, 2364–2376. [CrossRef]
30. Chen, S.; Zhang, L.; Zhang, C.; Huang, M. Experimental study on the seepage characteristics of bituminous coal under the conditions of liquid nitrogen fracturing. *Energy Sci. Eng.* **2019**, *7*, 2138–2154. [CrossRef]
31. Du, M.; Gao, F.; Cai, C.; Su, S.; Wang, Z. Study on the surface crack propagation mechanism of coal and sandstone subjected to cryogenic cooling with liquid nitrogen. *J. Nat. Gas Sci. Eng.* **2020**, *81*, 103436. [CrossRef]
32. Li, H.; Dong, Z.; Ouyang, Z.; Liu, B.; Yuan, W.; Yin, H. Experimental investigation on the deformability, ultrasonic wave propagation, and acoustic emission of rock salt under triaxial compression. *Appl. Sci.* **2019**, *9*, 635. [CrossRef]
33. Su, S.J.; Gao, F.; Cai, C.Z.; Du, M.L.; Wang, Z.K. Effect of low temperature damage on tensile strength of coal under the liquid nitrogen freezing. *Therm. Sci.* **2020**, *24*, 3979–3986. [CrossRef]
34. Akhondzadeh, H.; Keshavarz, A.; Al-Yaseri, A.Z.; Ali, M.; Awan, F.U.R.; Wang, X.; Yang, Y.F.; Iglauer, S.; Lebedev, M. Pore-scale analysis of coal cleat network evolution through liquid nitrogen treatment: A micro-computed tomography investigation. *Int. J. Coal Geol.* **2020**, *219*, 103370. [CrossRef]
35. Zhang, L.; Chen, S.; Zhang, C.; Fang, X.; Li, S. The characterization of bituminous coal microstructure and permeability by liquid nitrogen fracturing based on μCT technology. *Fuel* **2020**, *262*, 116635. [CrossRef]
36. Zhang, H.; Wang, D.; Yu, C.; Wei, J.; Liu, S.; Fu, J. Microcrack evolution and permeability enhancement due to thermal shocks in coal. *PLoS ONE* **2020**, *15*, e0232182. [CrossRef] [PubMed]
37. Lin, H.; Li, J.; Yan, M.; Li, S.; Qin, L.; Zhang, Y. Damage caused by freeze-thaw treatment with liquid nitrogen on pore and fracture structures in a water-bearing coal mass. *Energy Sci. Eng.* **2020**, *8*, 1667–1680. [CrossRef]
38. Qin, L.; Li, S.; Zhai, C.; Lin, H.; Zhao, P.; Shi, Y.; Bai, Y. Changes in the pore structure of lignite after repeated cycles of liquid nitrogen freezing as determined by nitrogen adsorption and mercury intrusion. *Fuel* **2020**, *267*, 117214. [CrossRef]
39. Li, B.; Ren, Y.; Lv, X. The evolution of thermal conductivity and pore structure for coal under liquid nitrogen soaking. *Adv. Civ. Eng.* **2020**, *2020*, 2748092. [CrossRef]
40. Liu, S.; Li, X.; Wang, D.; Zhang, D. Investigations on the mechanism of the microstructural evolution of different coal ranks under liquid nitrogen cold soaking. In *Energy Sources, Part A: Recovery, Utilization, and Environmental Effects*; Taylor & Francis: Oxfordshire, UK, 2020; pp. 1–17.
41. Akhondzadeh, H.; Keshavarz, A.; Awan, F.U.R.; Ali, M.; Al-Yaseri, A.; Liu, C.; Yang, Y.; Iglauer, S.; Gurevich, B.; Lebedev, M. Liquid nitrogen fracturing efficiency as a function of coal rank: A multi-scale tomographic study. *J. Nat. Gas Sci. Eng.* **2021**, *95*, 104177. [CrossRef]
42. Sun, Y.; Zhai, C.; Xu, J.; Cong, Y.; Zheng, Y. Experimental study on pore structure evolution of coal in macroscopic, mesoscopic, and microscopic scales during liquid nitrogen cyclic cold-shock fracturing. *Fuel* **2021**, *291*, 120150. [CrossRef]
43. Shao, Z.; Ye, S.; Tao, S.; Feng, X.; Wang, Y. Experimental study of the effect of liquid nitrogen penetration on damage and fracture characteristics in dry and saturated coals. *J. Pet. Sci. Eng.* **2021**, *201*, 108374. [CrossRef]
44. Lin, H.F.; Long, H.; Yan, M.; Li, S.G.; Shu, C.M.; Bai, Y. Methane adsorption thermodynamics of coal sample subjected to liquid nitrogen freezing–thawing process. *J. Nat. Gas Sci. Eng.* **2021**, *90*, 103896. [CrossRef]
45. Liu, S.; Li, X.; Wang, D.; Zhang, D. Experimental study on temperature response of different ranks of coal to liquid nitrogen soaking. *Nat. Resour. Res.* **2021**, *30*, 1467–1480. [CrossRef]
46. Qin, L.; Wang, P.; Li, S.; Lin, H.; Wang, R.; Wang, P.; Ma, C. Gas adsorption capacity changes in coals of different ranks after liquid nitrogen freezing. *Fuel* **2021**, *292*, 120404. [CrossRef]

47. Sun, Y.; Zhao, Y.; Li, Y.; Danesh, N.N.; Zhang, Z. Characteristics Evolution of Multiscale Structures in Deep Coal under Liquid Nitrogen Freeze-Thaw Cycles. *Geofluids* **2021**, *2021*. [CrossRef]
48. Yang, Y.; Liu, S.; Chang, X. Fracture stiffness evaluation with waterless cryogenic treatment and its implication in fluid flowability of treated coals. *Int. J. Rock Mech. Min. Sci.* **2021**, *142*, 104727. [CrossRef]
49. Qin, L.; Ma, C.; Li, S.; Lin, H.; Wang, P.; Long, H.; Yan, D. Mechanical damage mechanism of frozen coal subjected to liquid nitrogen freezing. *Fuel* **2022**, *309*, 122124. [CrossRef]
50. Yuan, Y.; Cai, F.; Yang, L. Pore structure characteristics and fractal structure evaluation of medium-and high-rank coal. *Energy Explor. Exploit.* **2022**, *40*, 328–342. [CrossRef]
51. Akhondzadeh, H.; Keshavarz, A.; Awan, F.U.R.; Zamani, A.; Iglauer, S.; Lebedev, M. Coal cleat network evolution through liquid nitrogen freeze-thaw cycling. *Fuel* **2022**, *314*, 123069. [CrossRef]
52. Li, C.; Nie, B.; Feng, Z.; Wang, Q.; Yao, H.; Cheng, C. Experimental Study of the Influence of Moisture Content on the Pore Structure and Permeability of Anthracite Treated by Liquid Nitrogen Freeze–Thaw. *ACS Omega* **2022**, *7*, 7777–7790. [CrossRef]
53. Cai, C.; Gao, F.; Yang, Y. The effect of liquid nitrogen cooling on coal cracking and mechanical properties. *Energy Explor. Exploit.* **2018**, *36*, 1609–1628. [CrossRef]
54. Qin, L.; Zhai, C.; Liu, S.; Xu, J. Mechanical behavior and fracture spatial propagation of coal injected with liquid nitrogen under triaxial stress applied for coalbed methane recovery. *Eng. Geol.* **2018**, *233*, 1–10. [CrossRef]
55. Yin, G.; Shang, D.; Li, M.; Huang, J.; Gong, T.; Song, Z.; Deng, B.; Liu, C.; Xie, Z. Permeability evolution and mesoscopic cracking behaviors of liquid nitrogen cryogenic freeze fracturing in low permeable and heterogeneous coal. *Powder Technol.* **2018**, *325*, 234–246. [CrossRef]
56. Cong, Y.; Zhai, C.; Sun, Y.; Xu, J.; Tang, W.; Zheng, Y. Visualized study on the mechanism of temperature effect on coal during liquid nitrogen cold shock. *Appl. Therm. Eng.* **2021**, *194*, 116988. [CrossRef]
57. Yang, R.; Hong, C.; Huang, Z.; Wen, H.; Li, X.; Huang, P.; Liu, W.; Chen, J. Liquid nitrogen fracturing in boreholes under true triaxial stresses: Laboratory investigation on fractures initiation and morphology. *SPE J.* **2021**, *26*, 135–154. [CrossRef]
58. Du, M.; Gao, F.; Cai, C.; Su, S.; Wang, Z. Experimental Study on the Damage and Cracking Characteristics of Bedded Coal Subjected to Liquid Nitrogen Cooling. *Rock Mech. Rock Eng.* **2021**, *54*, 5731–5744. [CrossRef]
59. Yang, R.; Hong, C.; Huang, Z.; Song, X.; Zhang, S.; Wen, H. Coal breakage using abrasive liquid nitrogen jet and its implications for coalbed methane recovery. *Appl. Energy* **2019**, *253*, 113485. [CrossRef]
60. Yao, B.; Wang, L.; Patterson, T.; Kneafsey, T.J.; Yin, X.; Wu, Y. Experimental study and modeling of cryogenic fracturing treatment of synthetic rock samples using liquid nitrogen under tri-axial stresses. In Proceedings of the SPE Unconventional Resources Conference, Calgary, AB, Canada, 15–16 February 2017.
61. Cong, Y.; Zhai, C.; Sun, Y.; Xu, J.; Tang, W.; Zheng, Y.; Zhu, X.; Yang, L. Study on transient boiling heat transfer of coal with different bedding angles quenched by liquid nitrogen. *Case Stud. Therm. Eng.* **2021**, *28*, 101463. [CrossRef]
62. Ma, H.; Zhu, C.; Zhao, P.; Wang, B. Freezing method for rock cross-cut coal uncovering: Aging characteristic of effective freezing distance on injecting liquid nitrogen into coal seam. *Adv. Civ. Eng.* **2021**, *2021*. [CrossRef]
63. Wen, H.; Yang, R.; Huang, Z.; Hu, X.; Hong, C.; Song, G. Flow and heat transfer of nitrogen during liquid nitrogen fracturing in coalbed methane reservoirs. *J. Pet. Sci. Eng.* **2022**, *209*, 109900. [CrossRef]
64. McDaniel, B.W.; Grundmann, S.R.; Kendrick, W.D.; Wilson, D.R.; Jordan, S.W. Field applications of cryogenic nitrogen as a hydraulic fracturing fluid. In Proceedings of the SPE Annual Technical Conference and Exhibition, San Antonio, TX, USA, 5–8 October 1997.
65. Wilson, D.R.; Siebert, R.M.; Lively, P. Conoco Inc. Cryogenic Coal Bed Gas Well Stimulation Method. U.S. Patent 5,464,061, 7 November 1995.
66. Zhang, L.; Ren, S.; Fan, Z.; Luo, J.; Che, H.; Yang, Y. Method of Low-Temperature Gas-Assisted Coalbed Methane Fracturing Technology. Chinese Patent CN103726819A, 24 June 2016.
67. Shen, C.; Zhang, L.; Wang, D.; Guo, J.; Gao, X.; Zhang, H.; Hou, J.; Jiang, L. Liquid Nitrogen Freeze-Thawing Cracking Coal-Bed Permeability-Increasing Coal-Bed Gas Mining Method. Chinese Patent CN104963660A, 24 October 2017.
68. Shen, C.; Zhang, L.; Wang, D.; Shu, L.; Guo, J.; Gao, X.; Zhang, H.; Qi, Q. Low Permeability Coal Bed Liquid Nitrogen Freeze Thawing Cracking Permeability Increasing Method. Chinese Patent CN104963674A, 2 March 2018.
69. Zhai, C.; Qin, L.; Xu, J.; Yu, G.; Sun, Y.; Dong, R.; Wu, S. A Kind of Method of the Anti-Reflection Coal Body Extraction Coal Bed Gas of Cycle Pulse Formula Low Temperature Freeze Thawing. Chinese Patent CN106337672B, 16 November 2018.
70. Xu, H.; Xin, F.; Wang, Q.; Wei, H.; Liu, D. Test Device and Test Method for Simulating Liquid Nitrogen Injection Freeze-Drying for Increasing Coal Bed Gas Yield. Chinese Patent CN103726819A, 27 September 2020.